REPORT No. 49

BOUNDARY LAYER ON AN AIRFOIL IN A CASCADE

CARL R. PETERSON

December, 1958

GAS TURBINE LABORATORY
MASSACHUSETTS INSTITUTE OF TECHNOLOGY
CAMBRIDGE · 39 · MASSACHUSETTS

BOUNDARY LAYER ON AN AIRFOIL IN A CASCADE

by

CARL R. PETERSON

Under the sponsorship of:

General Electric Company
Allison Division of General Motors Corporation
Westinghouse Electric Corporation

Gas Turbine Laboratory
Report Number 49

December
1958

Massachusetts Institute of Technology

ACKNOWLEDGEMENTS

This report was originally the authors master's thesis. The author would like to express his gratitude to all those who assisted on this project. The advice and guidance of Professors A. H. Stenning, the thesis adviser, and E. S. Taylor kept the work moving towards the proper end. The considerable assistance of Mr. Stephen Montgomery is especially appreciated.

The joint efforts of Mr. Basil Kean and Mr. Herbert Johnston produced the probe. Mr. Dalton Baugh produced nearly everything else as it was necessary.

Natalie Appleton did the typing.

ABSTRACT

A study of the turbulent boundary layer on an airfoil in a cascade is presented. The major portion of the observations are on the suction surface of the airfoil. The effect of added diffusion across the cascade due to a three-dimensional flow is included. Empirical equations describing the boundary layer in terms of momentum and displacement thickness growth as a function of free-stream diffusion are developed. Shape factor is also related to free-stream diffusion. A reasonable check with an existing separation criterion is observed. An appendix contains a discussion of chord-wise integrating of various boundary layer parameters.

TABLE OF CONTENTS

LIST OF FIGURES

TABLES

LIST OF SYMBOLS

l	distance from leading edge to minimum pressure point
p	pressure
u	velocity in boundary layer
x	chordal distance from leading edge
y	normal distance from surface of airfoil
H	shape factor
U	free-stream velocity
δ	boundary layer thickness (to u/U = .99)
δ^*	displacement thickness
θ	momentum thickness
ν	kinetic viscosity

Subscripts

max	maximum value
o	stagnation value
s	local static value
R_l	theoretical (Blasius) values based on l Reynolds number
∞	far from a flat plate or upstream of the cascade (refer to static pressure)

Identification of cascade conditions:

Example: 2D - 55 - 40 - S

First Group - without screen (2D), or with screen (3D)

Second Group - cascade angle

Third Group - percent chord

Last Letter - suction (S) or pressure (P) surface

DEFINITIONS

Cascade angle	angle between normal to cascade and flow direction (stagger angle = 45°)
Shape factor, H	$H \equiv \delta^*/\theta$
Displacement thickness	$\delta^* \equiv \int_0^\delta (1 - \frac{u}{U}) dy$
Momentum thickness	$\theta \equiv \int_0^\delta \frac{u}{U}(1 - \frac{u}{U}) dy$

BOUNDARY LAYER ON AN AIRFOIL IN A CASCADE

INTRODUCTION

In predicting the performance of turbomachine blading, two-dimensional cascade data is generally used, although the flow is not two-dimensional. The radial distribution of axial velocity may change across a blade row. In order to satisfy continuity, this causes a deviation of streamlines from a cylindrical pattern, as shown in the following sketch.

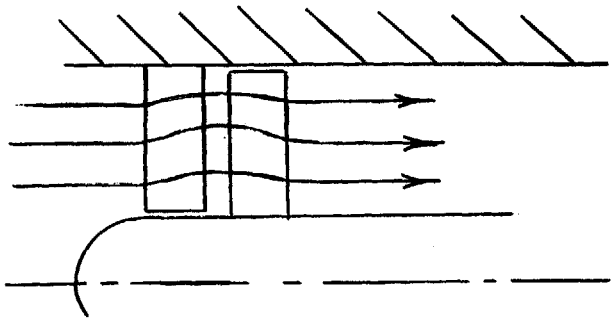

As can be seen, this in effect imposes an added diffusion near one end of the blades.

As part of an overall program investigating the effect of this added diffusion, the behavior of the boundary layer on the blade surface in such a region is here observed. The added diffusion is brought about

by placing an obstruction downstream of the span-wise centerline of a cascade. The centerline of symmetry then corresponds to one casing wall in the previous sketch, except that for this investigation it is free of the complications of wall friction.

DESCRIPTION OF APPARATUS

The Cascade

The investigations are being made on a newly constructed low speed wind tunnel. The tunnel construction allows continuous variation of inlet angle at constant cascade stagger over a wide range. The cascade consists of nine blades with 4 7/8 inch chord, 20 inch span, and NACA 65-410 section. The chord Reynolds number is roughly 3×10^5, corresponding to a velocity of 115 feet per second. The turbulence level has, as yet, not been determined, but it is known to be high.

For a complete discussion of the tunnel design and performance, see Gas Turbine Laboratory Report Number 43.

The Probe

One of the major objections to total pressure probes for use in boundary layer studies is one of physical size, as limited by reasonable response rates. The available pressure sensing apparatus allowed reasonable response rates even with the very small probe used. The very availability of this pressure sensing apparatus was a major factor in the choice of such a probe.

Another objection to the use of finite size total pressure probes is their behavior in a total pressure gradient. It has been shown that the displacement effect caused by such a gradient is exactly off-set by the interference effect as such a probe approaches a wall (1). Thus no correction of the data was necessary, either for pressure gradient or for wall effects. There is an interferance effect between a hotwire and a wall so that the total pressure probe appears to be advantageous in this respect.

The probe used was a three-hole cobra probe with tip dimensions .018 x .054 inches. The probe design and calibration are discussed in detail in the appendix.

Pressure Sensing Apparatus

The pressure was sensed by a Dynisco pressure transducer of $\pm$.10 psi range. Another such transducer of $\pm$.050 psi range is available for yaw determination. The unbalance of a bridge circuit containing the transducer is amplified by a D.C. amplifier produced by the Dynamic Instrument Company, Cambridge, Massachusetts. The bridge is balanced, as indicated by a galvamometer, with a potentiometer in the circuit - the potentiometer reading then being a measure of the pressure. The apparatus was calibrated against an NACA micromanometer, and found to be linear over the entire range of allowable pressures. The calibration has been repeated on subsequent occasions and the constant of proportionality found to vary less than one percent.

Blade static pressures were determined on a sloping manometer board containing 31 tubes. The inaccuracies due to non-flat boards and non-uniform tubes were minimized by careful construction and selective assembly. The slope of the board and the specific gravity of the manometer oil are such that five inches of oil on the board are equal to one inch of water.

EXPERIMENTAL PROCEEDURE

The added diffusion over a central portion of the span was produced by an eight inch perforated metal screen placed four inches (perpendicular to the cascade) downstream of the blade trailing edges as shown below. The perforations are 1/8 inch diameter holes giving a screen of 40% open area.

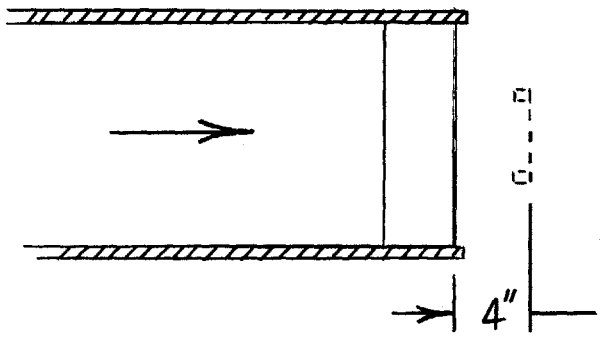

The choice of screen size, geometry, etc., and its effects on the flow are covered in detail in Gas Turbine Laboratory Report Number 48.

Whenever possible, tests were made at constant velocity as determined by the difference in static pressures between a position just upstream of the cascade and the plenum. Velocity was varied by the adjustment of a bleed slot, downstream of the fan. For cascade angles of 52° and 56°, with the screen in place, the velocity could not be maintained at 115 feet per second, even with the bleed slot fully closed.

Cascade angle was determined by a scale fixed directly to the cascade support structure.

It was desired to obtain boundary layer traverses at several chord positions, on both sides of the blade, for several cascade angles,

with and without the downstream screen. This was first broken into two cases - with and without the screen. Following this, since the most difficult probe adjustment was that of chord position, the data was taken at each chord position for all cascade angles before moving to the next chord position. All chord positions except 60% chord were reached from the rear mounting position of the probe (see appendix for description of probe mechanism). The 60% position was reached from the forward mounting position. Chord position was determined by measuring from the trailing edge of the blade with an ordinary steel scale. After taking data without the screen, the procedure was repeated unchanged for the cases with the screen in position.

As outlined in the appendix, the change of probe-to-blade distance could be determined with high precision. It was also necessary to determine one fixed probe position from which to measure all changes. In the final procedure this was taken as the contact position - that is, with the probe in contact with the blade surface. Each traverse was started at the outer limit of the traverse range and continued in to the blade surface. As the tip approached the blade the position increments were decreased. Pressure readings were taken at each position until no change in pressure could be observed for a supposed change in tip position. This meant that the tip was in contact with the blade, and was not actually changing position. In regions of steady flow and steep pressure gradient this was an extremely precise means of determining the contact position. For unsteady regions or flat pressure gradients (near the trailing edge at high cascade angles) the technique was not good. However, it was nearly always possible to determine the contact position at a low angle

of attack and use this information for the high angle of attack, since the runs were made consecutively. It was found that the contact position did not vary appreciably for two runs at the same chord position. When it was not possible to run an unsteady traverse in conjunction with a steady one it was necessary to determine contact position visually. This resulted in only a slight loss in accuracy, but a great loss in convenience.

The range of probe traverse was limited by the wedge dimensions to slightly less than .30 inches. When readings at greater distance were necessary the probe position was determined visually with gauge blocks, using one of the adjustments mentioned in the appendix to extend the probe range.

RESULTS

Data

Figures 4 and 5 show the observed values of momentum thickness, displacement thickness, and actual thickness (to u/U = .99). Actual thickness was read directly from plots of u/U versus y since the velocity gradients were such that it could be done with little uncertainty. Momentum and displacement thicknesses were found by graphical integration of the appropriate areas.

Figures 6 through 9 show typical velocity profiles plotted on a dimensionless basis. Attempts to plot all chord position curves on one graph result in confusion, since the curves are very close together, but not close enough to be considered one curve. Hence, complete velocity profile data is presented in Table I. The unsteady readings shown are not a true measure of flow unsteadiness since the probe response was so slow. They are a measure of the relative unsteadiness from one run to another, however.

Figure 9 is of particular interest, since it shows an obviously separated flow, although the exact shape of the profile near the wall can only be estimated. The total pressure probe read a steady, low value in the back-flow region. The probe tip was reversed (pointed downstream) in this region, and the total pressure was then observed to be a little higher. This indicated simply that there actually was a back flow. The pressure readings could not have quantitative value, however, since the probe tip was reading in the wake of its own support.

Frictionless Analysis

In some cases it has been possible to analyze the outer portion of boundary layers on a frictionless basis. In this analysis, the outer portion of a boundary layer is approximated by a series of stream tubes, each of constant velocity. Bernoulli's equation, together with the known static pressure distribution, and the continuity equation are then sufficient to describe the downstream development of a given portion of the profile. This analysis was applied in two cases in an attempt to predict the 80 and 98% chord profiles, given the 60% profile and the static pressure distribution. The analysis was found invalid.

Correlations

As with most complex phenomena, empirical correlation methods are necessary for quantitative description of gross boundary layer behavior. Two parameters are of primary interest; the momentum thickness and the displacement thickness.

The development of a boundary layer between any point on an airfoil and some other point downstream might be expected to be a function of the following:

1) Free-stream diffusion over the interval
2) Boundary layer characteristics at the upstream position
3) Skin friction over the interval

The diffusion may be expressed as the free-stream velocity ratio over the interval. The upstream characteristics may be expressed

in terms of the preceding parameters. A simple plot of momentum thickness, θ, versus free-stream velocity ratio U/U_{max}, results in a good correlation, indicating that skin friction is not an important variable.

Momentum Thickness

To make the experimental results more generally applicable it is desirable to normalize the momentum thickness in the above plot with some length characteristic of the flow. As observed by others (3), the most significant length for this purpose is the momentum thickness at the minimum pressure point, since it may be assumed that transition from a laminar to turbulent boundary layer occurs here. This also accounts for the use of U_{max} as the significant velocity used in the correlation. Cobalt chloride tests and the static pressure distributions indicate that transition and the minimum pressure point both occur very near the leading edge (on the suction surface), but they do not precisely locate the position of either. It is therefore necessary to make assumptions regarding both the location of the minimum pressure point and the momentum thickness at this point.

For those cases in which the minimum pressure point occurred farther than 1.7% of the chord from the leading edge, the location and magnitude of the minimum pressure could be determined with some certainty. For cases in which the minimum pressure occurred nearer the leading edge it was assumed that it occurred at 1.7% chord, and that its magnitude was that value measured at the 1.7% pressure tap. With this imformation it is possible to compute U_{max}, or at least a good approximation to it.

The minimum pressure point momentum thickness must be calculated,

since it is impossible to determine experimentally. Since the boundary layer is laminar up to the minimum pressure point, one might assume Blasius flat-plate flow to calculate the momentum thickness.

Then: $$\theta = .664\sqrt{\nu x/U_\infty}$$

and $$\theta_{R_l} = .664\sqrt{\nu l/U_\infty}$$

where x is the surface distance from the leading edge, and l is the x distance to the minimum pressure point. Due to the curvature of the airfoil, x or l is not actually equal to chordal distance, but for these calculations it may be assumed so. The actual value of U varies from zero at the stagnation point to U_{max} at the minimum pressure point. U_{max} is of the order of twice the upstream U so a mean U may reasonably be taken as the upstream U. With these assumptions, θ_{R_l} may be calculated.

The characteristic length must satisfy one further condition: as U/U_{max} approaches one, θ must approach the characteristic length. It was empirically found that $2\theta_{R_l}$ satisfied this last condition. In Figure 1 the resulting correlation of $\theta/2\theta_{R_l}$ versus U/U_{max} is shown. The data fits the following empirical equation quite well:

$$\frac{\theta}{2\theta_{R_l}} = \left[\frac{U_{max}}{U}\right]^5 \qquad (1)$$

for

$$\frac{U}{U_{max}} > .51$$

The exponent, 5, has been observed by others (3).

The factor, 2, while quite arbitrary, is only slightly more arbitrary than the use of θ_{R1}. θ_{R1} is significant only in that it is probably a function of the proper variables, ν, x, and U_∞. The actual flow is far from flat-plate flow, and even if it were not, the Blasius solution does not apply near a leading edge (6).

The actual flow probably included laminar separation followed by reattachment as a turbulent boundary layer. Transition occurs, on a flat-plate at least, for x Reynolds numbers ($U_\infty x/\nu$) of from 3×10^5 to 3×10^6 (6). The actual x Reynolds numbers were of the order of $.4 \times 10^4$ to 1.4×10^4, based on chordal distance and upstream velocity. Hence, transition must have been the result of separation and reattachment.

Reference 3 contains a means of calculating the limiting possible energy recovery without separation in the form of the following emperical equation:

$$E_{LIM} = 1 - \left[\frac{U_2}{U_{max}}\right]^2 = 1 - 3.24\left[\frac{\theta_1}{L}\right]^{.324}$$

where U_2 = free-stream velocity at point of incipient separation

θ_1 = minimum pressure point momentum thickness

L = length of pressure rise

In the present case

$$\theta_1 = 2\theta_{R1}$$

Looking at the three-dimensional, 60° cascade angle case as the only example of sharp separation, it may be seen from the static pressure or velocity profile data that separation occurs at approximately 70% chord.

Then:

$$L \cong 3.5 \text{ inches}$$

With these figures in the above equation

$$\frac{U}{U_{max}} \cong .52$$

From Figure 1, this is seen to be in agreement with the point where the momentum thickness increases very rapidly with decreasing U/U_{max}.

Due to the unusual pressure distribution on the pressure surfaces, these correlations can not be expected to apply.

Displacement Thickness

The same type of correlation may be ma with displacement thickness. Again, for the Blasius flow:

$$\delta^* = 1.73\sqrt{\nu x/U_\infty}$$

or

$$\delta^*_{R_L} = 2.61\,\theta_{R_L} \qquad (2)$$

It was not necessary to use an arbitrary multiple of δ^* to bring the displacement thickness ratio to one as the velocity ratio approached one. There is no reason to expect that a similar factor should appear in the δ^* and θ correlations, for if it did, it would indicate that the actual shape factor at the minimum pressure point was equal to the Blasius shape factor. In this particular case, at the minimum pressure point:

$$H \equiv \frac{\delta^*}{\theta} = \frac{\delta^*_{R_L}}{2\theta_{R_L}} = \frac{1}{2} H_{R_L} \cong 1.3$$

This shape factor is characteristic of a flat-plate turbulent boundary layer.

The resulting correlation, shown in Figure 2, gives the following equation:

$$\frac{\delta^*}{\delta^*_{R_1}} = \left[\frac{U_{max}}{U}\right]^{5.5} \tag{3}$$

In both Figures 1 and 2 it can be seen that two sets of data fall to the right of the curves, but parallel to it. Since the curves are of the same shape, an error in U/U_{max} is possible. These two sets of data are for the highest cascade angles for the two and three-dimensional flows. These correspond to the greatest uncertainty in U_{max}. The shift of the two sets of data corresponds to an error in U_{max} of less than ten percent. An error in U_{max} would be an underestimation, tending to shift the points in the observed direction.

Shape Factor

Equations (1), (2) and (3) may be combined to eliminate the Blasius parameters, resulting in the following:

$$H = \frac{\delta^*}{\theta} = \frac{1.305}{\sqrt{U/U_{max}}} \tag{4}$$

This equation and the corresponding experimental data are plotted in Figure 3. The equation is seen to be in excellent agreement with the data over the range $.51 < U/U_{max} < .81$. For $U/U_{max} < .51$ the flow is separated and equations (1) and (3) do not apply. Hence the data can be expected to deviate. The data for $U/U_{max} > .81$ corresponds to low cascade angles. In these cases transition may be taking place over

an appreciable distance rather than occurring suddenly at the minimum pressure point. Hence the shape factor may be expected to tend towards higher (laminar) values as U/U_{max} approaches one in these cases.

Conclusions

Two conclusions may be drawn from these correlations. First, as mentioned, the growth of the boundary layer is independent of x dimensions or skin friction. Second, the geometry of the diffusion, whether three-dimensional or two-dimensional, is not important. Both of these conclusions indicate that free-stream diffusion is the variable of primary importance in boundary layer development. The conclusions are, of course, drawn on relatively little data and are strictly valid only for the geometries investigated. They are, however, in general agreement with other observations.

The arbitrary nature of the Blasius parameters may be eliminated if it is desired to predict the subsequent development of a known parameter.

Hence,

$$\frac{\theta_a}{\theta_b} = \frac{\theta_a/2\theta_{R_1}}{\theta_b/2\theta_{R_1}} = \frac{\left[\frac{U_{max}}{U_a}\right]^5}{\left[\frac{U_{max}}{U_b}\right]^5}$$

$$\therefore \frac{\theta_a}{\theta_b} = \left[\frac{U_b}{U_a}\right]^5$$

The same is true for displacement thickness:

$$\frac{\delta_a^*}{\delta_b^*} = \left[\frac{U_b}{U_a}\right]^{5.5}$$

APPENDIX I

PROBE DESIGN AND CALIBRATION

Design

The probe used in this investigation was a three-hole cobra probe especially designed to satisfy the particular requirements encountered. These requirements may be stated in the form of the four criteria used in the probe design:

1) Small probe size

2) Flexibility of operating configuration

3) Rigid support for a given operating configuration

4) Accurate determination of probe tip position

A small probe tip was necessary in order to obtain a reasonable amount of data within the thin boundary layers anticipated. The probe tip was formed of three tubes of 0.018 inches outside diameter and 0.010 inches inside diameter silver-soldered together in the conventional cobra-probe configuration. None of the tubes was flattened. The included tip angle was 60° for maximum sensitivity (2). Reasonable response rates were obtained with such a probe tip by using a relatively rigid pressure sensing system of low volume. The probe was connected to Dynisco transducers with 18 inches of plastic tubing of approximately .025 inches inside diameter. This system responded to a step change in pressure of 2 inches of water in less than thirty seconds.

The carbon-black traces (Figure 15) show that the probe tip was well out of the wake of its own support mechanism. The probe probably altered the overall passage flow a little by its slight blockage of the

passage as may be seen in Figure 14. It is assumed that errors due to this effect are small.

Flexibility of operating configuration and rigid support in position are slightly conflicting criteria, although they can be realized simultaneously with careful workmanship. It was desired to use one probe tip to cover all positions on the airfoil, that is, all chord positions on both sides of the airfoil. Refering to Figure 11, different chord-wise positions are attained by sliding the horizontal slide forward or back on the cross support. The horizontal slide could be mounted as shown or reversed, that is, extending upstream from the cross support. When in the upstream position it is necessary to rotate the probe hanger 180° with respect to the horizontal slide at joint B. In any position the bottom of the probe could be made tangent to the airfoil by proper rotation at joint B. In order to span the entire chord it was necessary to provide two cross support holes and wedge guides in the airfoil. When switching from side to side of the airfoil (separate airfoils were used for each side) it is also necessary to rotate the probe tip 180° with respect to the probe hanger at joint A. This adjustment also allowed back-flow measurements with the probe tip facing downstream as mentioned in the text.

Rigidity in position is attained by insuring tight joints. Joint A is a tight friction joint, the probe tip lock being a split sleeve that fits tightly over the mating parts. The probe tip and probe hanger are shaped in such a way that they mate in only two position, 180° apart. Joint B is a carefully fitted friction joint. Due to the long slits in the horizontal slide it was necessary to provide a set-screw lock for the joint at C. Joint D is a pinned joint.

The traverse motion had to be both delicate and accurate, hence a screw and wedge combination with considerable mechanical reduction of motion was devised as shown in Figure 11. Contact between the wedge and the wedge contact pin was maintained by spring in the main probe support. Fine traverse adjustments were made by moving the wedge (slope of 10:1) vertically with the wedge traverse screw (40 threads per inch). Coarse position adjustment could be made by screwing the wedge contact pin in or out of the wedge block. Very coarse adjustments were made by moving the wedge block on the cross support, and holding it in position with a set-screw.

Calibration

In the final configuration, probe position was calibrated as a function of revolutions of the wedge traverse screw from some known position. The tip position was calibrated against a series of objects of known dimensions held against the airfoil, using the completion of an electrical circuit to determine contact. With care the calibration could be reproduced to within the uncertainty of the dimensions of the gauge objects (about .001 inches). It was necessary to calibrate the probe in this manner for each of the probe support locations. The probe tip position was a linear function of wedge traverse screw position over the entire range of about 0.28 inches on the suction side of the airfoil. It was linear for a range of only 0.15 inches on the pressure side where the calibration was carried on to a distance of 0.21 inches from the airfoil surface. The constants of proportionality over the linear portions differed by about 1.8% from one side to the other.

The probe's fluid dynamic characteristics were calibrated in a small wind tunnel in the Gas Turbine Laboratory. Uniform, steady flows over a velocity head range of .9 to 2.96 inches of water were attainable. The data for total pressure error versus angle of attack shown in Figure 12 indicates an error of less than one percent over a range of about sixteen degrees centered approximately on the probe axis. Scatter in the data indicates approach to the limiting sensitivity of the instrumentation rather than inconsistant probe performance.

It was intended that the probe should determine angle of attack by measuring the unbalance of pressure between the two outer tubes, rather than physically yawing out the probe. This latter method was, of course, impossible under the circumstances. Although the probe has not, as yet, been used to determine angles of flow, it has been calibrated to do so in the same wind tunnel mentioned above. The relationship between angle of attack and unbalance in pressure was found to be linear over a range of plus or minus sixteen degrees. The constant of proportionality showed a more or less random scatter of about one percent over the range of velocity heads mentioned above.

APPENDIX II

CHORD INTEGRATING TECHNIQUES

Reference 4 contains an analytical relation for wake momentum thickness and suction surface diffusion ratio for cascades of the type used in this investigation. The relation involves a particular chordwise integral of a function of shape factor, momentum thickness and free stream velocity which could not be evaluated directly. The present data allows a limited look at the validity of the integrating techniques employed in the approximate evaluation of the above integral.

The momentum equation for two-dimensional incompressible boundary layers (6),

$$\frac{\tau_0}{\rho} g_0 = \frac{d}{dx}(U^2\theta) + \delta^* U \frac{dU}{dx}$$

where τ_0 = wall shear stress

ρ = density

can be written in the form:

$$\frac{d\theta}{dx} = \frac{C_f}{2} - (H+2)\frac{\theta}{U}\frac{dU}{dx}$$

where

$$C_f = \frac{\tau_0}{\rho \frac{U^2}{2g_0}}$$

This can be integrated over the chord from x = 0 to x = c, the chord length. Thus,

$$\frac{1}{c}\theta_{te} = \frac{1}{c}\int_0^c \frac{C_f}{2} dx \quad - \frac{1}{c}\int_0^c (H+2)\frac{\theta}{U}\frac{dU}{dx} dx$$

where subscript te denotes trailing edge conditions and the equation is normalized on the chord length.

Attention is here devoted to evaluation of the final integral on the suction surface of the airfoil. The data indicates that we may assume U_{max} occurs at the leading edge. Thus the integral might be evaluated directly as follows:

$$-\frac{1}{c}\int_0^c (H+2)\frac{\theta}{U}\frac{dU}{dx}dx = \frac{1}{c}\int_{U_{te}}^{U_{max}} (H+2)\theta\frac{dU}{U}$$

The present data allows direct graphical evaluation of this integral, except that assumptions of the values θ and H at $U = U_{max}$ must be made. θ may be assumed equal to zero, as is actually the case at the leading edge, or equal to $2\theta_{R1}$, the value indicated at $U = U_{max}$ by the preceding work. The difference in the integrated result is negligible. The shape factor at the leading edge was taken as 1.3 as indicated in the preceding work. Again, the integration will decrease the effect of an error in this assumption.

Reference 4 makes a first approximation to this integral in the following manner, again assuming that U_{max} occurs at x = 0.

$$-\frac{1}{c}\int_0^c (H+2)\frac{\theta}{U}\frac{dU}{dx}dx \cong \overline{(H+2)(\theta/c)}\ln\left(\frac{U_{max}}{U_{te}}\right)$$

with the implied definition of $\overline{(H + 2)\ (\theta/c)}$:

$$\overline{(H+2)(\theta/c)} = \frac{1}{c}\int_0^c (H+2)(\theta/c)\,dx$$

This, of course, is true only if the averaged quantity is actually a constant. The data shows that it is far from constant.

A second approximation is made as follows:

$$\overline{(H+2)(\theta/c)} \cong (\overline{H}+2)\overline{(\theta/c)}$$

where $$\overline{H} = \frac{1}{c}\int_0^c H\,dx \quad ; \quad \overline{\theta} = \frac{1}{c}\int_0^c \theta\,dx$$

The above two approximations may also be graphically evaluated from the present data, and compared to the direct evaluation. The same assumptions are valid for H and θ at the leading edge. U_{max} was found as in the preceding work. U_{te} was taken as the free stream velocity at the 98% chord position.

With these assumptions, the various integrals were evaluated with the following results:

Run conditions	$\frac{1}{c}\int_{U_{te}}^{U_{max}}(H+2)\theta\frac{dU}{U}$	$\overline{(H+2)(\theta/c)}\ln\frac{U_{max}}{U_{te}}$	$(\overline{H}+2)\overline{(\theta/c)}\ln\frac{U_{max}}{U_{te}}$
2D - 56	.00218	.00189 (-13.6%)	.00721 (-66.9%)
2D - 62	.00715	.01137 (+59.0%)	.00739 (+3.4%)
2D - 65	.0146	.0272 (+86.3%)	.0167 (+14.4%)
3D - 52	.00400	.00311 (-22.2%)	.00226 (-43.5%)
3D - 56	.00857	.01063 (+24.0%)	.00696 (-18.8%)
3D - 60	.01292	.0373 (+189%)	.0217 (+68.2%)

Thus it is seen that the second approximation, which was the one used in Reference 4, is by chance the better one in all but the low angle of attack cases. It is in fair agreement with the direct evaluation at medium angles of attack and appears better for the two-dimensional flow cases.

The preceding integral approximation is a step in Lieblein's analysis and does not appear explicitly in his final correlation. The above discussion is, therefore, a look at the validity of a part of his analysis, rather than his final result.

BIBLIOGRAPHY

1) Davies, P. O. A. L.,

"The Behaviour of a Pitot Tube in Transverse Shear", Journal of Fluid Mechanics, Vol. 3, Part 5, February 1958, pp. 453-454.

2) Dean, R. C. Jr.,

"Aerodynamic Measurements", Gas Turbine Laboratory, M. I. T., 1953.

3) Jones, B. A.,

"Method for Prediction of Boundary Layer Separation and Growth for Application to Turbine-Blade Design", ASME Paper No. 57-F-30.

4) Lieblein, S.,

"Analytical Relation for Wake Momentum Thickness and Diffusion Ratio for Low-Speed Compressor Cascade Blades", NACA TN 4318, August 1958.

5) Montgomery, S. R.,

"The Design of a Low Speed Cascade Tunnel", Gas Turbine Laboratory Report No. 43, M. I. T., January 1958.

6) Schlichting, H.,

"Boundary Layer Theory", Pergamon Press, New York, 1955.

TABLE I

Velocity Profiles

y in inches

2D-55-20-S

y	u/U
.030	1.000
.022	.996
.018	.980
.017	.976
.016	.969
.015	.959
.014	.945
.013	.931
.012	.918
.012	.907
.011	.892
.010	.882
.009	.876

2D-55-20-P

.028	1.000
.019	.993
.015	.967
.012	.935
.010	.896
.009	.871

2D-55-40-S

.089	1.000
.067	.999
.046	.998
.037	.994
.033	.986
.029	.969
.024	.942
.020	.896
.016	.835
.012	.748
.009	.716

2D-55-40-P

.051	1.000
.043	.998
.034	.998
.025	.992
.021	.972
.016	.936
.012	.831
.010	.750
.009	.714

2D-55-60-S

.114	1.000
.092	.997
.071	.991
.050	.974
.028	.912
.020	.829
.011	.687
.010	.667
.009	.636

2D-55-80-S

.146	1.000
.125	.996
.103	.984
.082	.955
.060	.894
.039	.815
.030	.776
.022	.731
.018	.704
.013	.671
.012	.662
.012	.654
.010	.642
.009	.636

2D-55-80-P

.109	1.000
.087	.997
.066	.983
.055	.965
.044	.920
.035	.854
.026	.756
.022	.703
.018	.630
.013	.547
.011	.514
.009	.463

2D-55-90-S

.209	1.000
.166	.998
.145	.993
.123	.981
.102	.961
.080	.913
.059	.848
.038	.764
.021	.694
.016	.669
.012	.633
.010	.608
.009	.594

2D-55-90-P

.153	1.000
.131	.991
.109	.978
.087	.950
.070	.917
.061	.897
.053	.872
.044	.847
.035	.814
.026	.775
.022	.756
.018	.735
.013	.687
.009	.641

2D-55-98-S

.214	1.000
.172	.996
.150	.984
.129	.968
.107	.934
.086	.880
.065	.824
.043	.740
.035	.702
.026	.676
.018	.635
.013	.602
.011	.571
.009	.550

2D-55-98-P

.193	1.000
.153	.995
.131	.985
.109	.972
.087	.951
.066	.923
.057	.909
.048	.894
.040	.878
.031	.860
.022	.835
.016	.811
.013	.795
.011	.773
.009	.763

2D-62-20-S

.125	1.000
.103	.999
.082	.994

Table I continued

y	u/U
.060	.972
.039	.912
.030	.873
.022	.818
.013	.734
.012	.728
.009	.710
2D-62-20-P	
.028	1.000
.019	.992
.015	.978
.012	.939
.010	.920
.009	.888
2D-62-40-S	
.152	1.000
.131	.994
.109	.985
.088	.956
.066	.900
.045	.805
.028	.705
.019	.643
.015	.629
.011	.602
.009	.598
2D-62-40-P	
.025	1.000
.021	.992
.017	.972
.012	.907
.010	.858
.009	.754
2D-62-60-S	
.243	1.000
.200	.996
.157	.984
.136	.964
.114	.927
.093	.873
.071	.796
.050	.704
.029	.604
.020	.557
.016	.532
.012	.496
.010	.476
.009	.468
2D-62-80-S	
.309	.998
.296	.992
.253	.982
.210	.942
.167	.874
.125	.779
.082	.628
.060	.538
.039	.467
.022	.409
.018	.387
.013	.366
.010	.360
.009	.343
2D-62-80-P	
.066	1.000
.044	.970
.035	.918
.026	.778
.022	.690
.018	.560
.016	.493
.013	.442
.011	.375
.009	.307
2D-62-90-S	
.369	1.000
.349	.994
.329	.989
.309	.983
.311	.978
.294	.972
.251	.942
.208	.888
.166	.803
.144	.744
.123	.677
.101	.610
.080	.535
.059	.470
.037	.400
.020	.366
.012	.316
.009	.302
2D-62-90-P	
.108	1.000
.086	.988
.068	.966
.060	.944
.042	.891
.033	.852
.025	.800
.020	.774
.016	.741
.012	.686
.009	.649
2D-62-98-S	
.409	1.000
.389	.998
.369	.988
.349	.979
.329	.970
.309	.958
.299	.954
.282	.935
.265	.918
.248	.896
.235	.880
.214	.833
.192	.795
.171	.738
.149	.684
.128	.636
.107	.553
.085	.507
.064	.435
.042	.380
.025	.349
.017	.315
.012	.285
.011	.293
.009	.251
2D-62-98-P	
.153	1.000
.131	.998
.109	.991
.087	.974
.066	.953
.057	.938
.048	.920
.040	.905
.031	.886
.022	.859
.018	.851
.016	.832
.013	.817
.011	.794
.009	.791
2D-65-20-S	
.253	1.000
.232	.996
.210	.994
.189	.985
.189	.994
.167	.985
.167	.991
.146	.974
.146	.985
.125	.958
.125	.970
.103	.936
.103	.948
.082	.880
.082	.892
.060	.813
.060	.826
.043	.748
.043	.761
.035	.720
.035	.734
.026	.675
.026	.694
.022	.660
.022	.675
.020	.644
.020	.660
.018	.637
.018	.644
.015	.629
.015	.637
.013	.620
.013	.629
.011	.604
.011	.620
.009	.604
.009	.612
2D-65-40-S	
.459	.998
.459	1.000

Table I continued

y	u/U	y	u/U	y	u/U	y	u/U
.409	.997		.986		.953	.259	.421
.409	.999	.309	.958	.459	.922		.468
.359	.995		.974		.943	.304	.491
.359	.997	.294	.958	.409	.903		.527
.309	.991		.974		.922	.261	.400
.309	.996	.273	.940	.359	.860		.468
.300	.984		.958		.881	.218	.344
.300	.990	.230	.914	.309	.779		.400
.279	.978		.931		.825	.176	.283
.279	.984	.187	.878	.297	.791		.311
.236	.974		.904		.816	.133	.158
.236	.984	.144	.778	.233	.690		.243
.193	.962		.820		.729	.090	.205
.193	.974	.101	.678	.190	.588		.215
.150	.939		.714		.618	.073	.173
.150	.951	.080	.622	.147	.502		.195
.107	.879		.649		.539	.064	.158
.107	.892	.059	.561	.104	.396		.184
.086	.835		.574		.421	.056	.130
.086	.848	.042	.497	.083	.332		.158
.067	.789		.510		.377	.048	.089
.067	.802	.033	.460	.062	.288		.145
.048	.743		.475		.319	.039	.130
.048	.752	.024	.434	.045	.251	.030	.063
.039	.717	.020	.405		.274		.114
.039	.725		.414	.036	.243	.022	.000
.030	.702	.016	.383	.027	.226		.130
.030	.717		.389	.019	.207	.018	.000
.022	.671	.014	.383	.015	.198		.114
.022	.679	.012	.366	.012	.186	.008	.063
.018	.653		.361	.009	.176		
.018	.646	.010	.346			3D-52-20-S	
.013	.643		.356	2D-65-98-S			
.013	.648	.009	.341			.036	1.000
.011	.632			1.359	1.000	.028	.997
.011	.638	2D-65-80-S		1.159	.996	.024	.984
.009	.620				.992	.021	.982
.009	.625	1.009	1.000	.959	.974	.018	.958
		.909	.990		.985	.016	.933
2D-65-60-S			.996	.809	.952	.014	.903
		.809	.986		.963	.012	.856
.609	1.000		.992	.559	.862	.010	.801
.509	.992	.709	.980		.884	.009	.791
	.995		.986	.459	.763		
.459	.992	.609	.968		.814	3D-52-40-S	
	.997		.978	.409	.678		
.409	.983	.549	.962		.720	.061	1.000
	.989		.972	.359	.633	.044	.998
.359	.977	.509	.943		.663	.036	.994

Table I continued

y	u/U
.027	.976
.018	.896
.014	.797
.012	.715
.010	.653
.009	.639
3D-52-60-S	
.107	1.000
.086	.994
.065	.976
	.980
.056	.962
	.971
.048	.941
	.949
.039	.913
	.923
.030	.867
	.874
.022	.790
	.793
.013	.687
.010	.634
	.613
.009	.598
3D-52-80-S	
.190	1.000
.147	.994
.125	.985
.104	.964
.083	.921
	.928
.061	.844
	.850
.044	.772
.036	.740
.027	.694
.018	.654
.014	.616
.010	.576
.009	.560
3D-52-98-S	
.277	1.000
.255	.996
.234	.996
.191	.989
.148	.937
.127	.900
.105	.843
.084	.772
.063	.683
.045	.624
.037	.592
.028	.560
.020	.494
.015	.463
.012	.420
.010	.410
.009	.381
3D-56-20-S	
.092	1.000
.071	.989
.049	.960
	.967
.036	.932
	.939
.028	.910
	.918
.019	.868
	.875
.015	.826
	.834
.013	.804
	.812
.012	.785
	.789
.010	.754
.009	.748
3D-56-40-S	
.147	1.000
.104	.995
.083	.981
.061	.940
	.946
.044	.871
	.879
.036	.835
	.847
.027	.789
	.799
.018	.738
	.746
.014	.701
	.707
.011	.665
	.669
.009	.641
3D-56-60-S	
.257	1.000
.236	.998
.193	.998
.150	.989
.129	.977
	.978
.107	.946
	.956
.086	.899
	.910
.065	.820
	.831
.056	.787
	.796
.048	.732
	.753
.039	.683
	.702
.030	.660
	.667
.022	.612
	.623
.013	.565
.011	.536
.009	.507
3D-56-80-S	
.296	1.000
.274	.992
	1.000
.232	.974
	.985
.189	.940
	.956
.146	.860
	.877
.125	.790
	.808
.103	.714
	.753
.082	.627
	.658
.060	.527
	.580
.043	.468
	.499
.035	.437
	.468
.026	.402
	.437
.018	.365
	.387
.013	.349
	.357
.009	.323
3D-56-98-S	
.509	1.000
.409	.982
	.996
.369	.971
	.985
.339	.952
	.964
.309	.945
	.933
.300	.910
	.930
.278	.870
	.910
.235	.811
	.841
.193	.697
	.746
.150	.592
	.638
.128	.500
	.560
.107	.439
	.486
.086	.396
	.414
.064	.317
	.348

Table I continued

y	u/U	y	u/U	y	u/U	y	u/U
.047	.246	.319	.994	.150	.636		.245
.039	.246		.998		.689	.104	.105
.030	.246	.297	.984	.129	.595		.164
.021	.207		.990		.636	.083	.105
.013	.170	.275	.980	.107	.508		.164
.009	.027		1.000		.532	.061	.071
		.232	.961	.086	.461	.044	.071
3D-60-20-S			.980		.487	.036	.071
		.190	.955	.065	.376	.027	.071
.286	1.000		.967		.433	.018	.000
.244	.997	.147	.913	.048	.341	.014	.000
.222	.996		.926		.376	.010	.000
.201	.996	.104	.820	.039	.266	.009	.000
.179	.996		.832		.310		
.158	.982	.083	.750	.030	.257	3D-60-98-S	
	.989		.769		.285		
.137	.975	.061	.673	.022	.237	1.109	.979
	.982		.688	.013	.226		1.000
.116	.954	.044	.610	.011	.200	1.059	.979
	.968		.624	.009	.187		.987
.094	.910	.036	.559			.909	.940
	.925		.566	3D-60-80-S			.966
.072	.856	.027	.524			.809	.882
	.872		.540	1.009	1.000		.896
.051	.764	.018	.485	.909	.986	.709	.821
	.772		.489		.992		.867
.038	.727	.014	.449	.809	.981	.609	.738
	.736		.454		.992		.805
.030	.689	.011	.417	.709	.948	.509	.623
	.698	.009	.398		.964		.702
.025	.676			.509	.814	.459	.558
	.680	3D-60-60-S			.676		.623
.023	.664			.409	.730	.389	.426
	.675	.509	.993		.766		.534
.021	.658		1.000	.369	.655	.349	.359
	.664	.459	.988		.611		.426
.019	.645		.995	.339	.616	.309	.323
	.652	.409	.961		.676		.359
.017	.632		.972	.309	.594	.299	.278
	.637	.369	.940		.634		.323
.015	.615		.966	.297	.526	.278	.228
	.621	.329	.918		.594		.323
.012	.599		.946	.275	.500	.235	.160
	.606	.289	.888		.571		.278
.010	.592		.916	.232	.417	.192	.000
	.597	.257	.847		.472		.167
.009	.588		.874	.190	.303	.149	.000
		.236	.817		.383		.123
3D-60-40-S			.859	.147	.266	.107	.071
		.193	.756		.303	.021	.000
.409	.998		.788	.125	.182	.012	.000
						.009	.000

TABLE II

Free Stream Dynamic Pressures

Cascade angle	$p_o - p_\infty$ (inches of water)
2D-55	2.97
2D-62	3.00
2D-65	2.99
3D-52	2.50
3D-56	2.55
3D-60	2.69

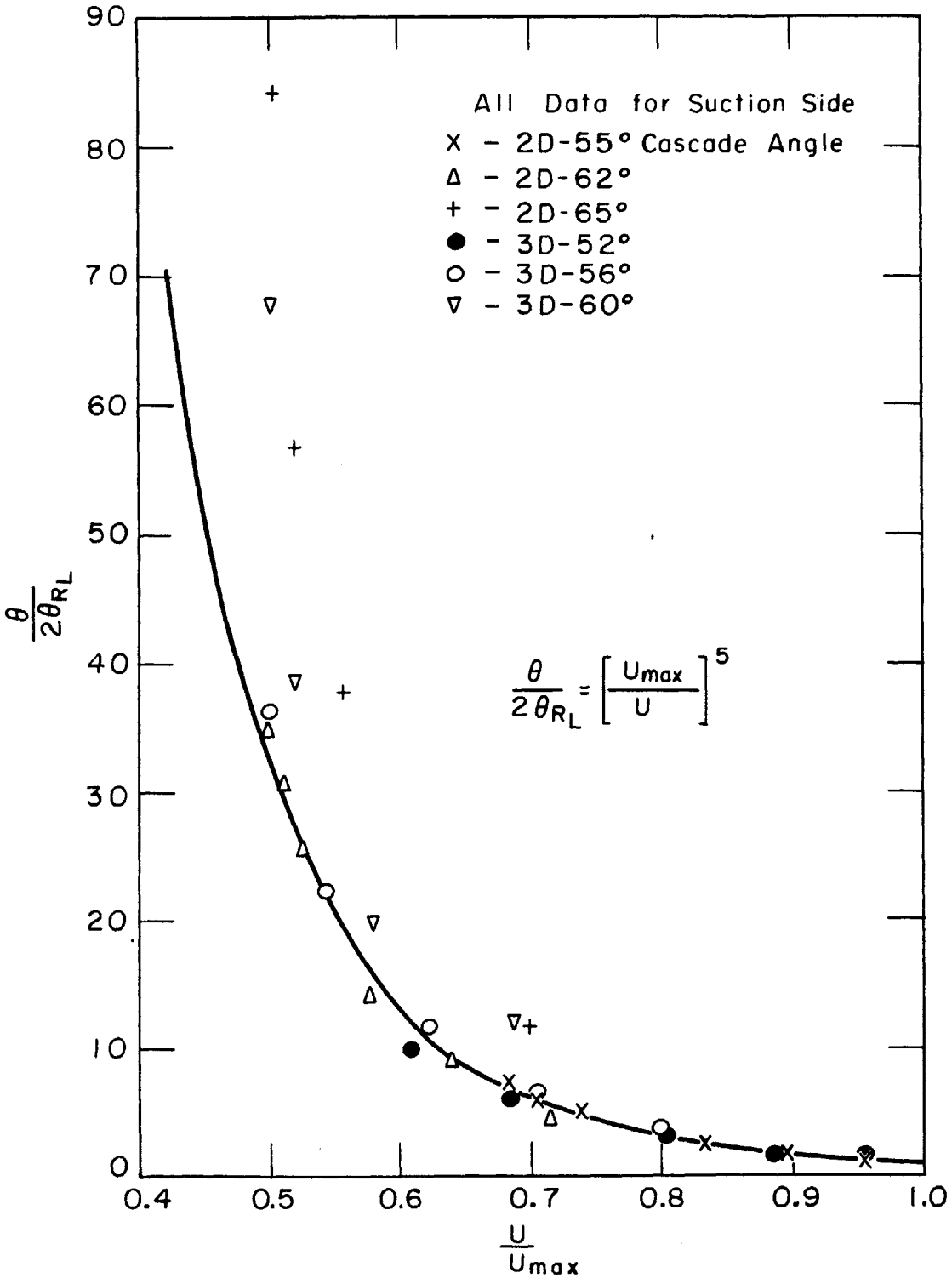

MOMENTUM THICKNESS CORRELATION

FIG. 1

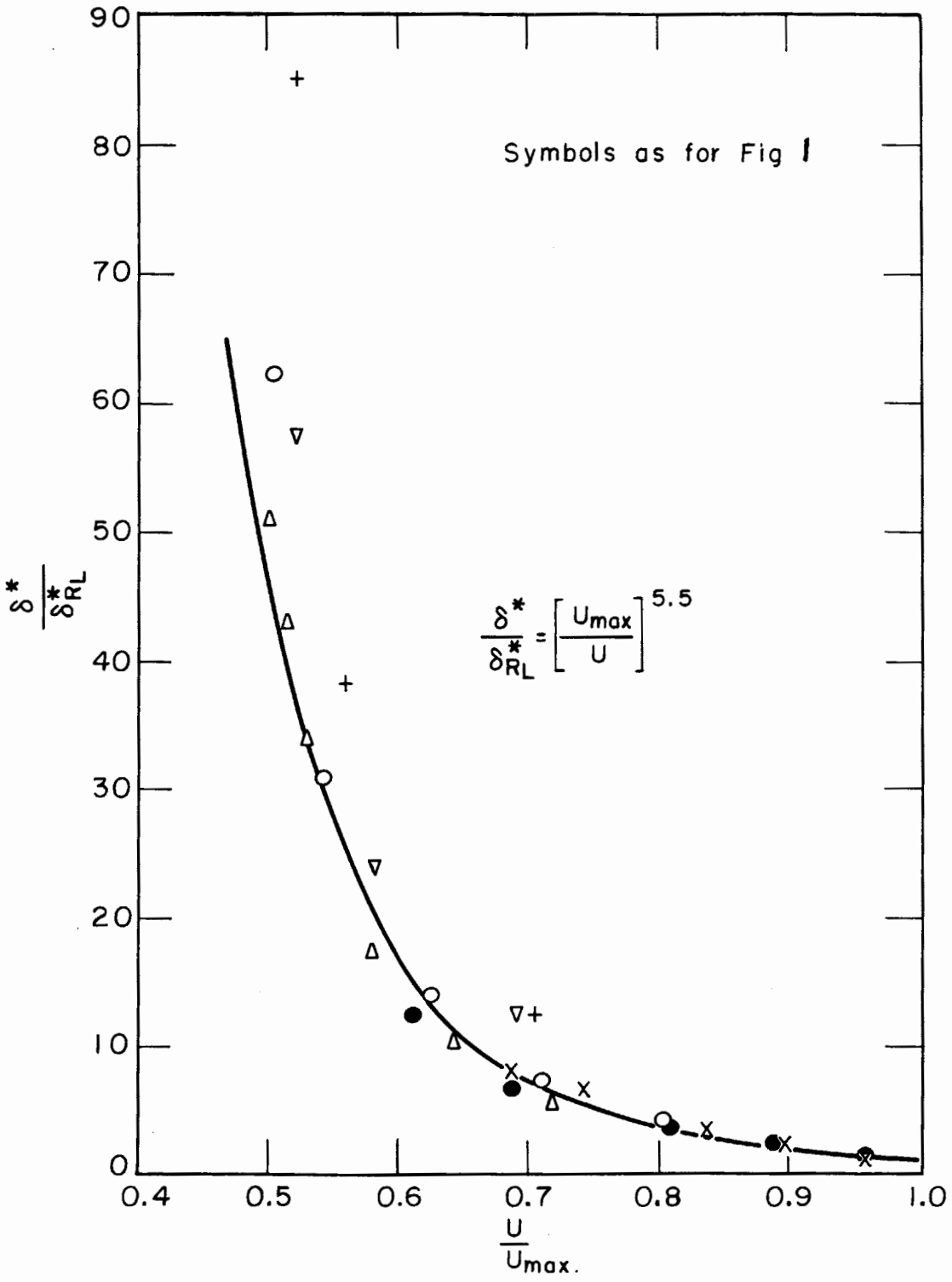

DISPLACEMENT THICKNESS CORRELATION

FIG. 2

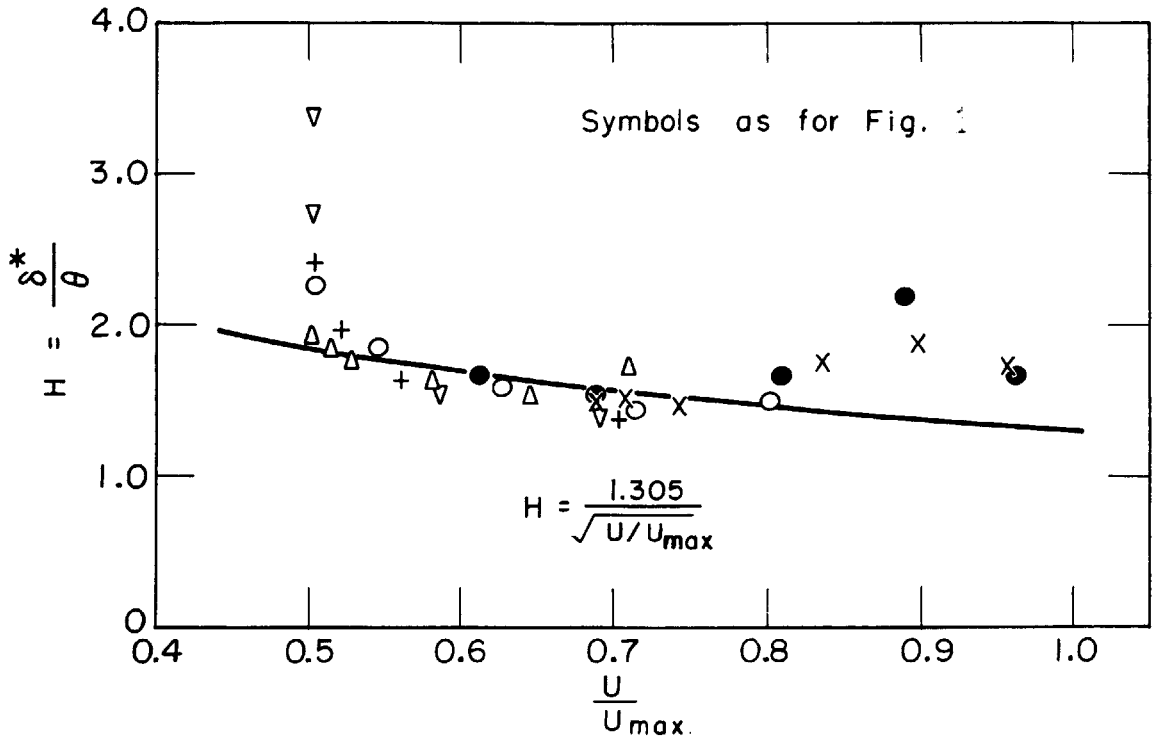

SHAPE FACTOR CORRELATION

FIG. 3

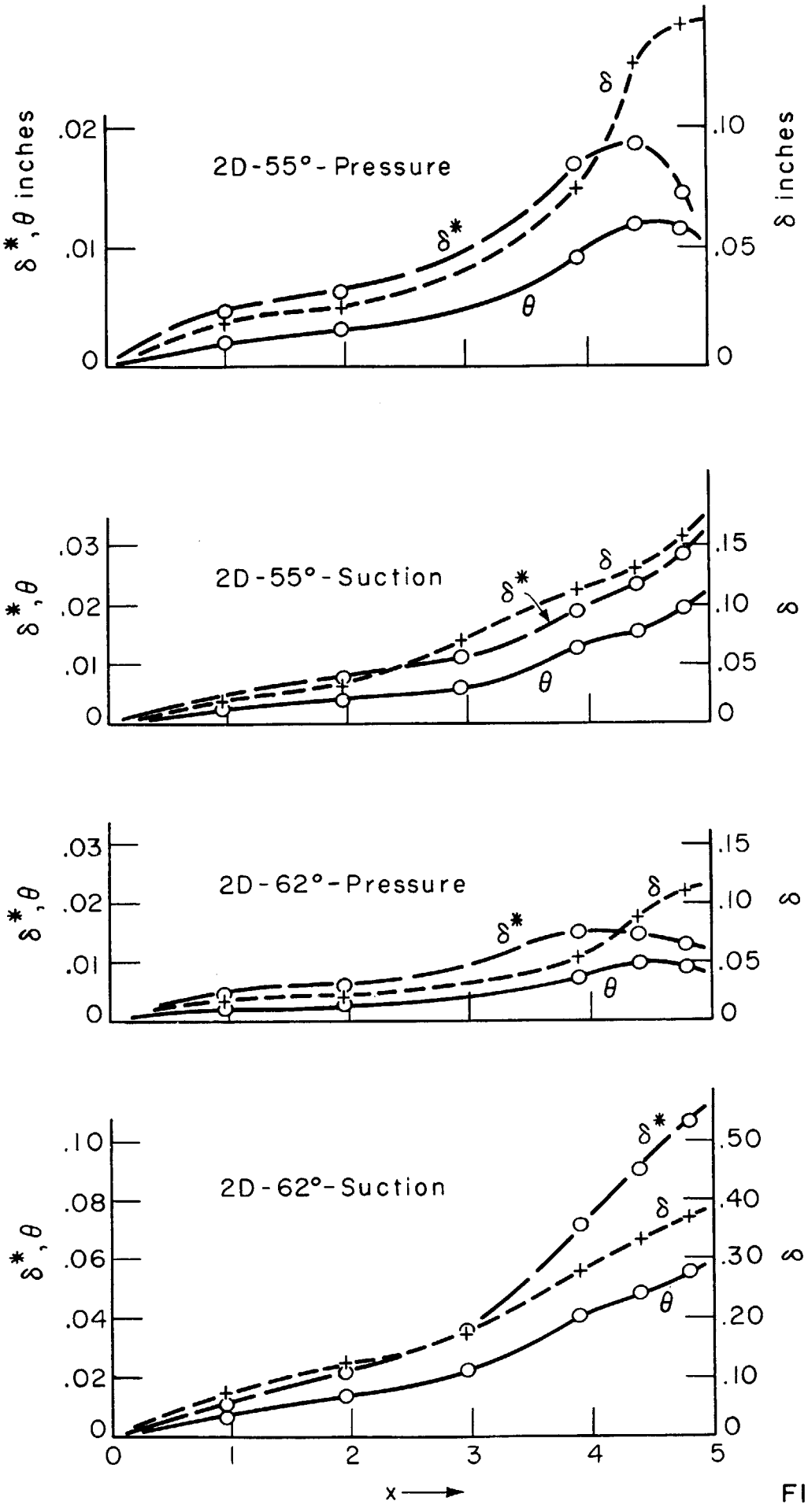
2D-55°-Pressure
δ*,θ inches
δ inches
δ*
θ
δ
2D-55°-Suction
2D-62°-Pressure
2D-62°-Suction
x

FIG. 4

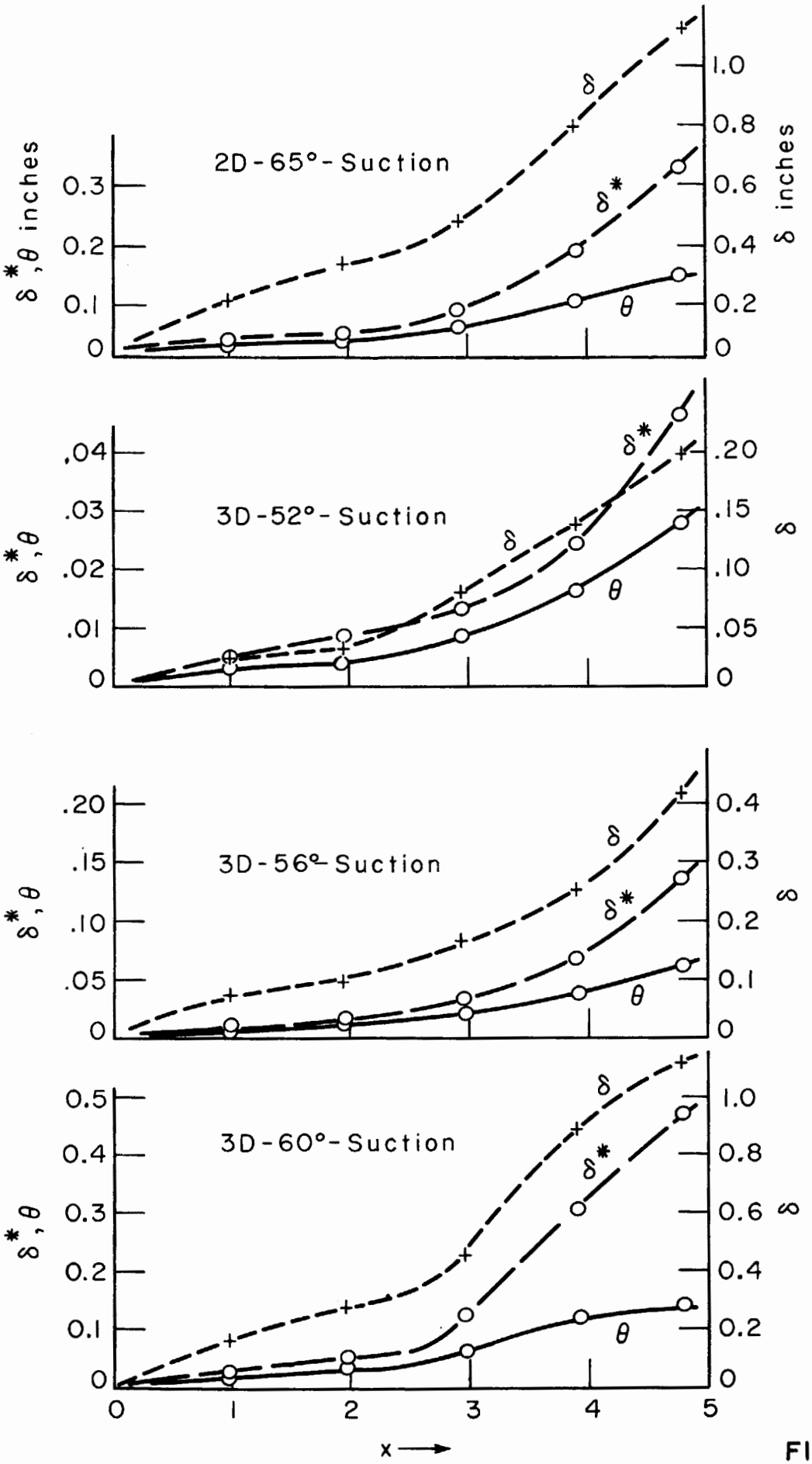
2D-65°-Suction
3D-52°-Suction
3D-56°-Suction
3D-60°-Suction
δ*,θ inches
δ inches
δ
δ*
θ
x

FIG. 5

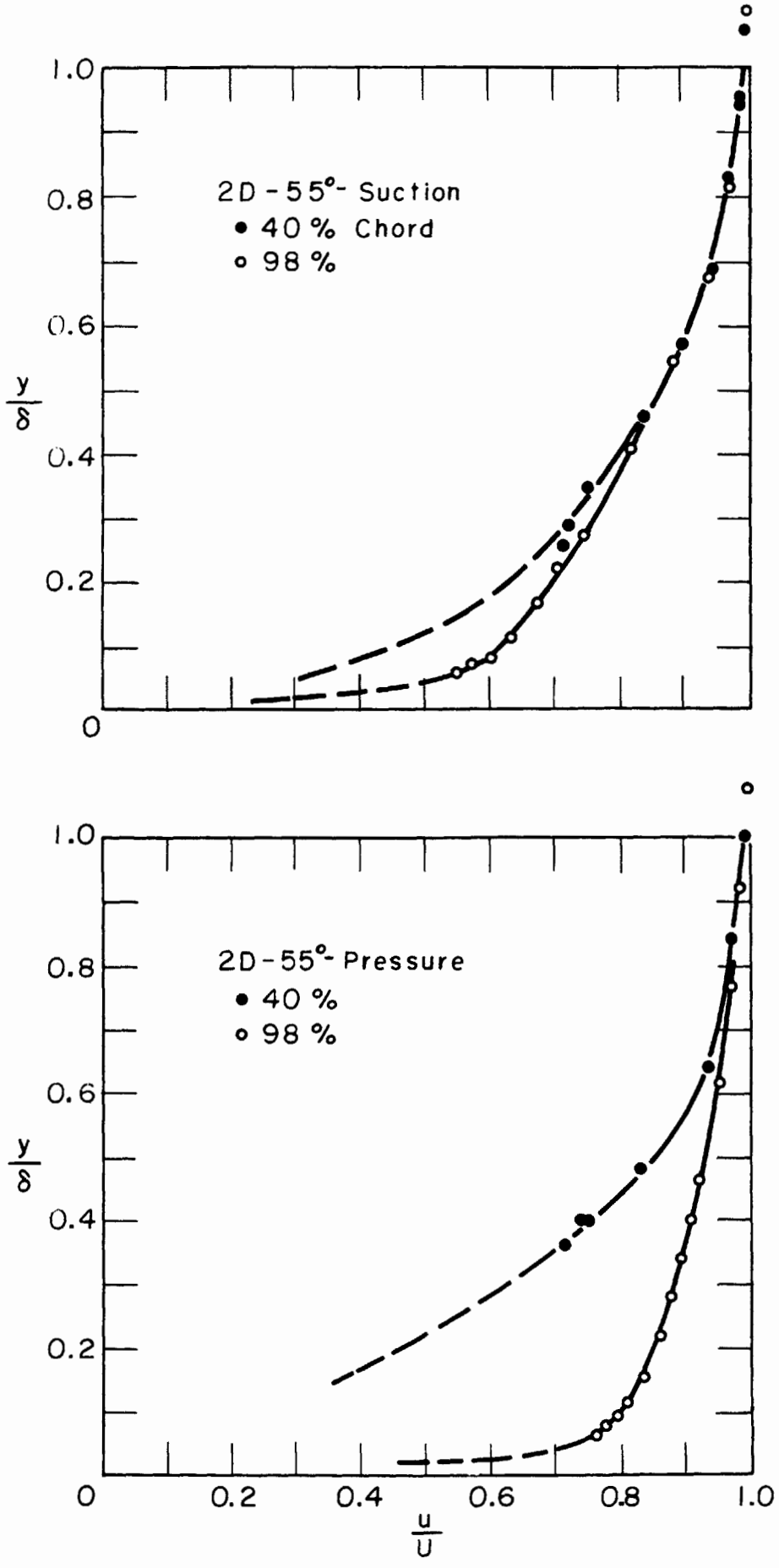
2D - 55°- Suction
• 40 % Chord
∘ 98 %
y/δ
1.0
0.8
0.6
0.4
0.2
0

2D - 55°- Pressure
• 40 %
∘ 98 %
y/δ
1.0
0.8
0.6
0.4
0.2
0
0.2
0.4
0.6
0.8
1.0
u/U

FIG. 6

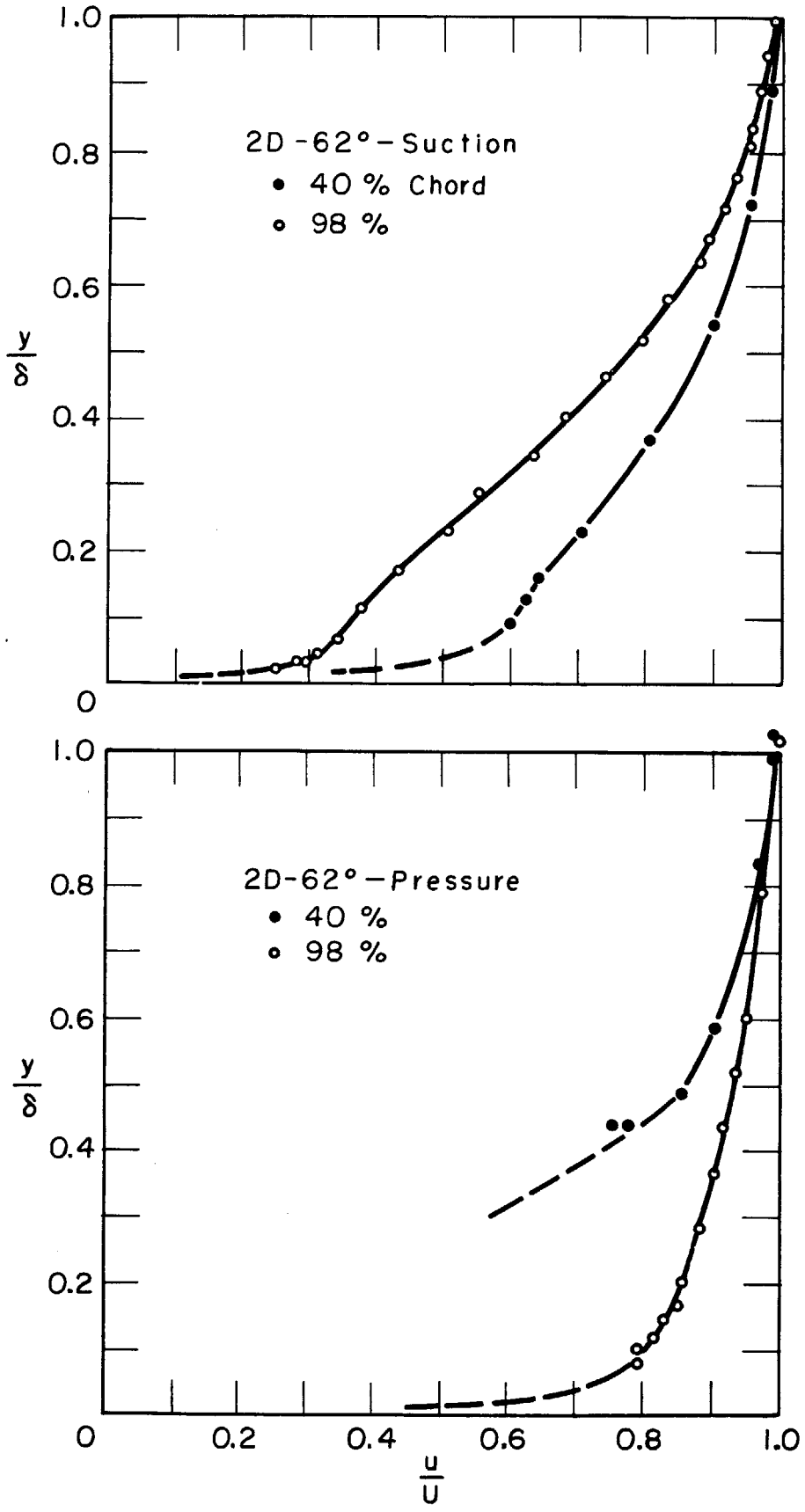
2D -62° – Suction
• 40 % Chord
∘ 98 %
2D-62° – Pressure
• 40 %
∘ 98 %
y/δ
u/U
0
0.2
0.4
0.6
0.8
1.0

FIG. 7

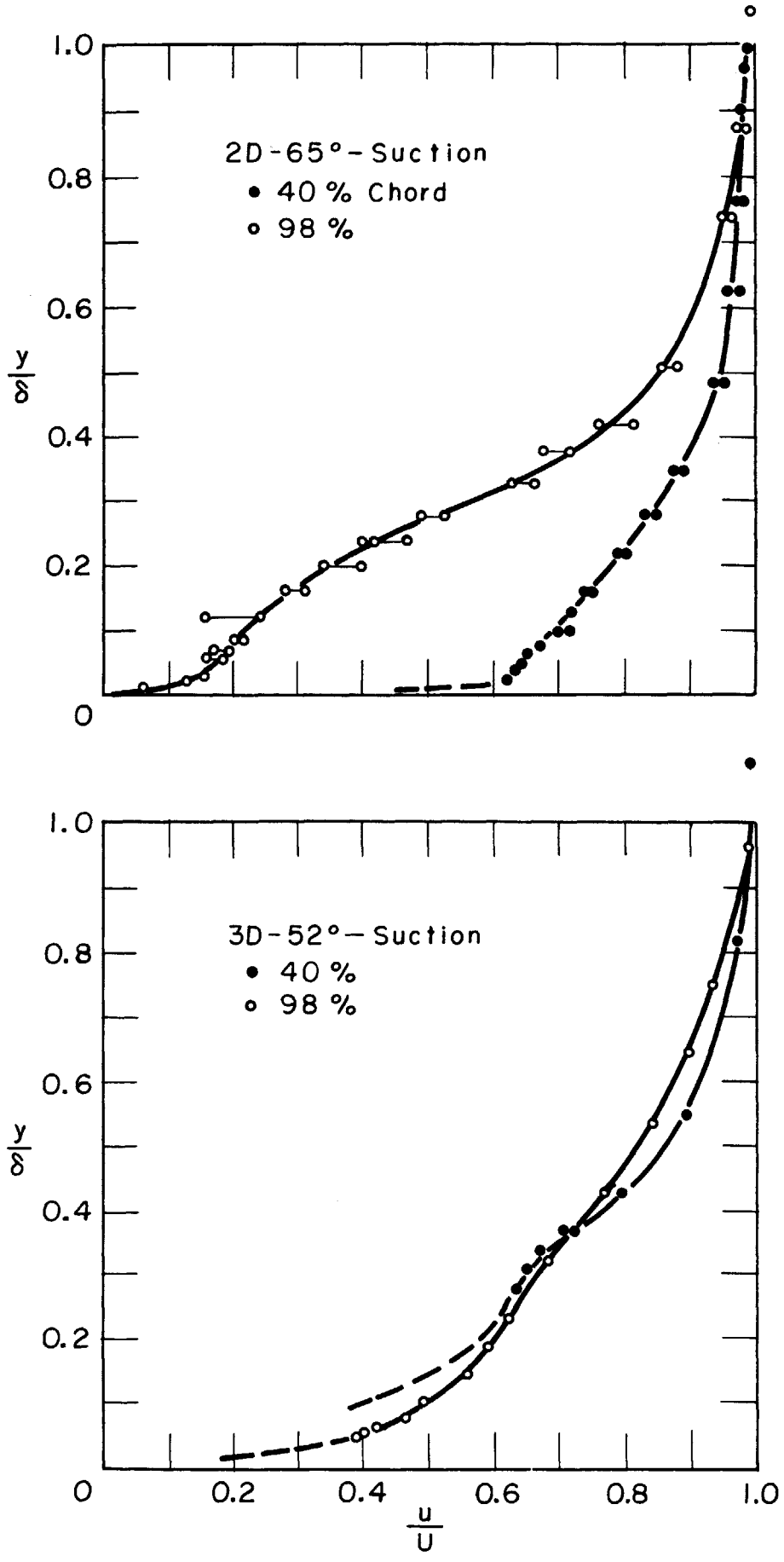
2D-65°-Suction
• 40 % Chord
○ 98 %
3D-52°-Suction
• 40 %
○ 98 %
y/δ
u/U
0
0.2
0.4
0.6
0.8
1.0

FIG. 8

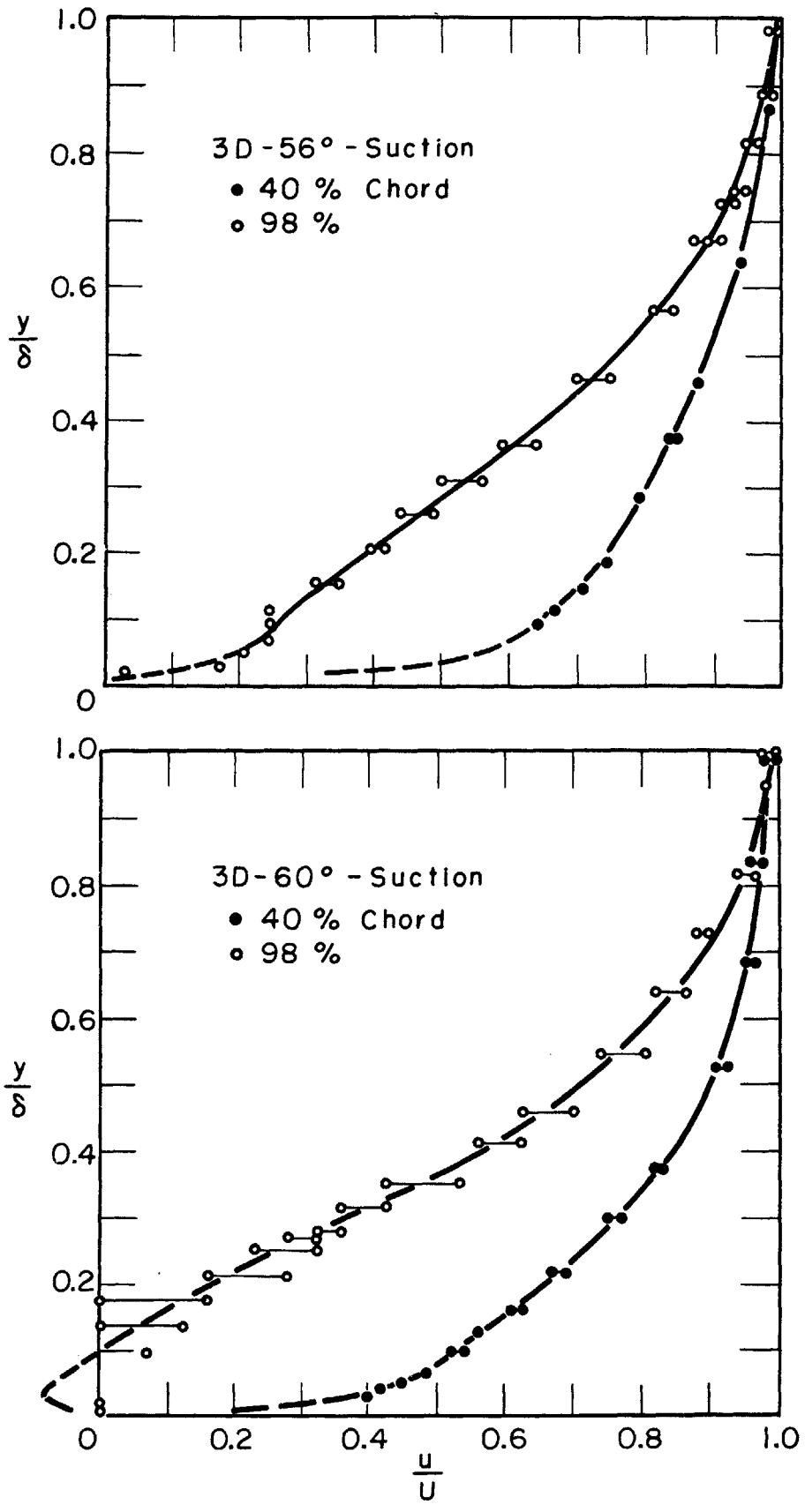
3D-56° - Suction
• 40 % Chord
○ 98 %
3D-60° - Suction
• 40 % Chord
○ 98 %
y/δ
u/U
0
0.2
0.4
0.6
0.8
1.0

FIG. 9

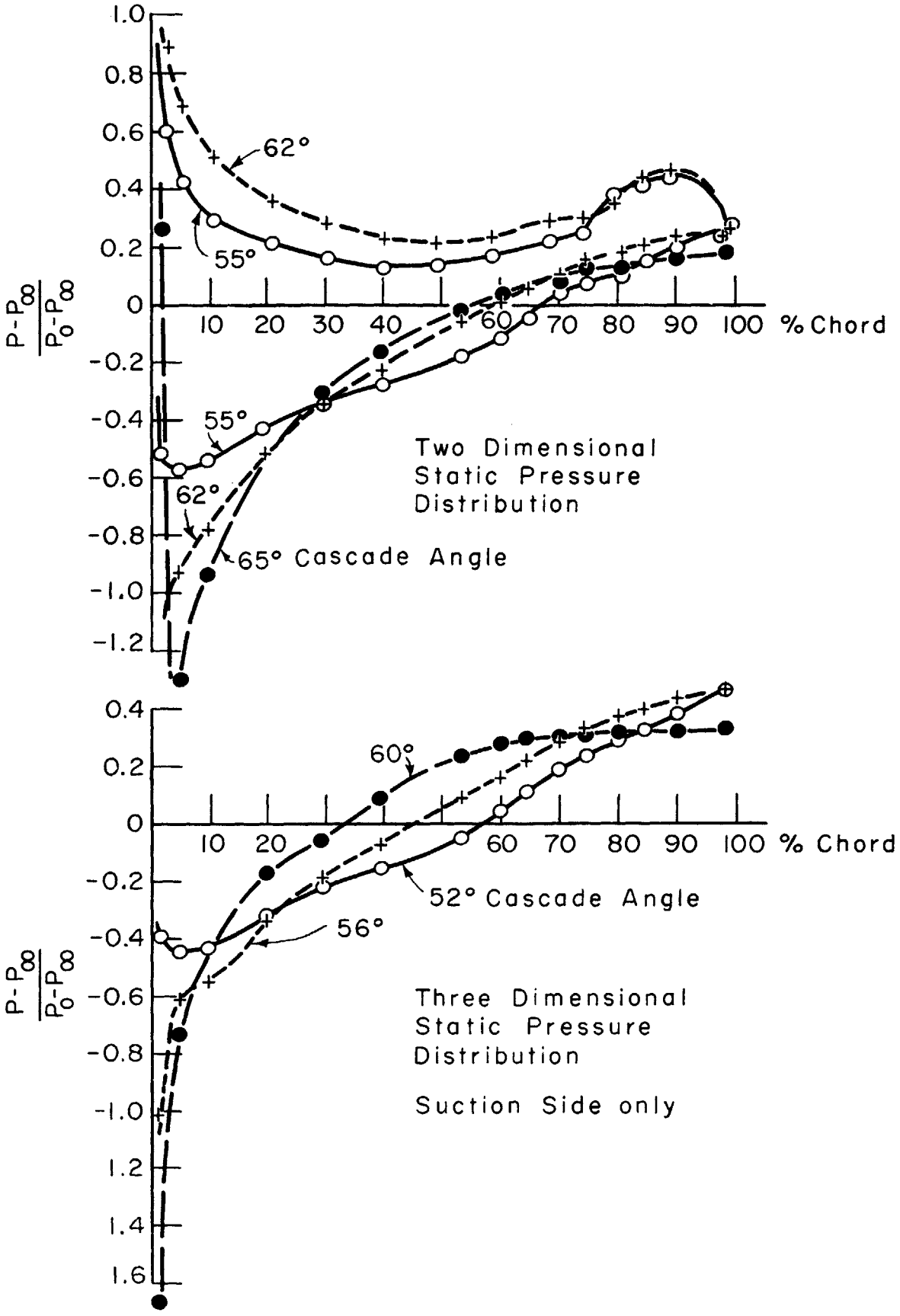
1.0
0.8
0.6
0.4
0.2
0
-0.2
-0.4
-0.6
-0.8
-1.0
-1.2
62°
55°
10 20 30 40 60 70 80 90 100 % Chord
$\frac{P-P_\infty}{P_0-P_\infty}$
55°
62°
65° Cascade Angle
Two Dimensional
Static Pressure
Distribution
0.4
0.2
0
-0.2
-0.4
-0.6
-0.8
-1.0
1.2
1.4
1.6
60°
10 20 60 70 80 90 100 % Chord
52° Cascade Angle
56°
$\frac{P-P_\infty}{P_0-P_\infty}$
Three Dimensional
Static Pressure
Distribution
Suction Side only

FIG. 10

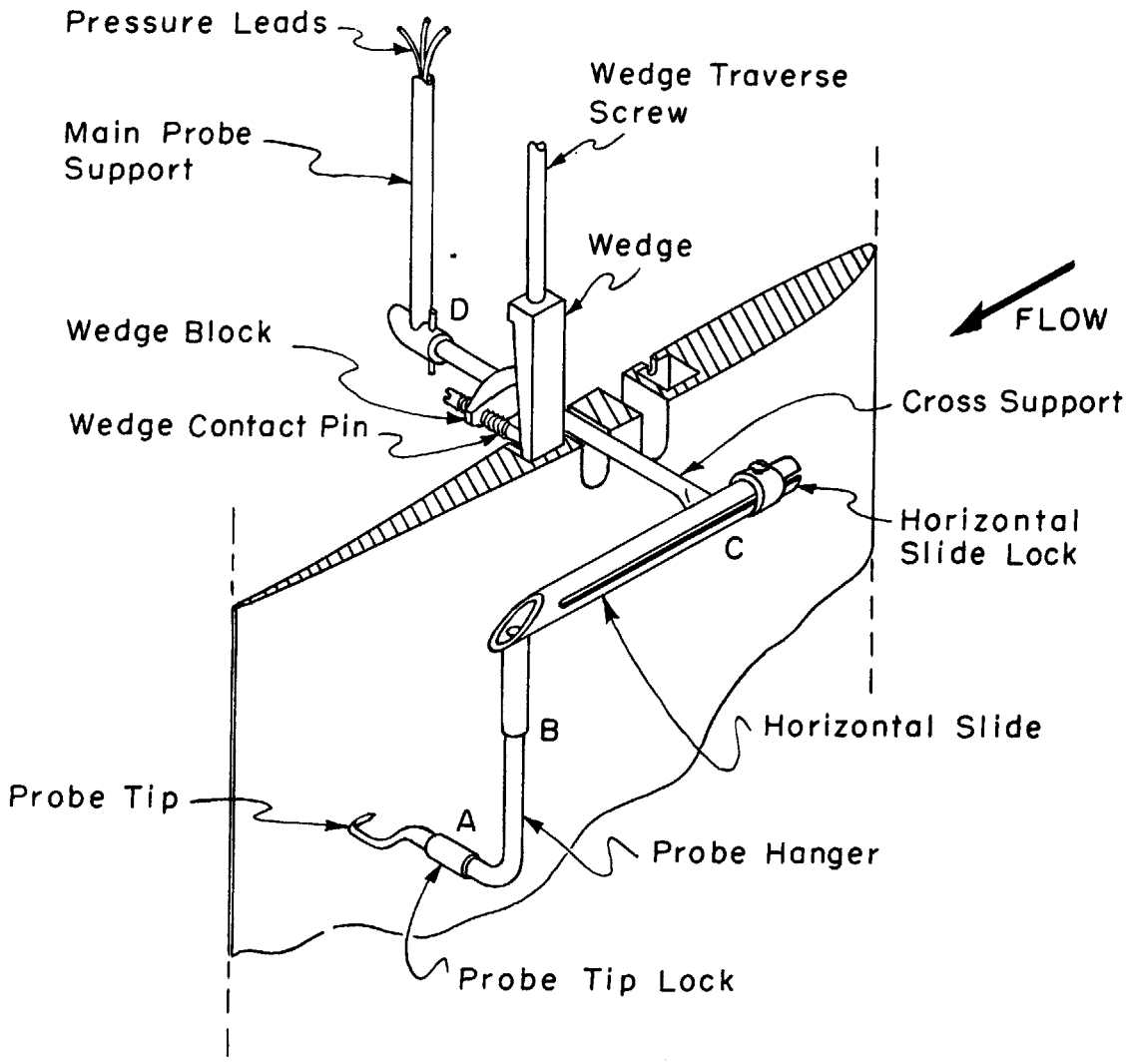

FIG. 11 BOUNDARY LAYER TRAVERSE PROBE

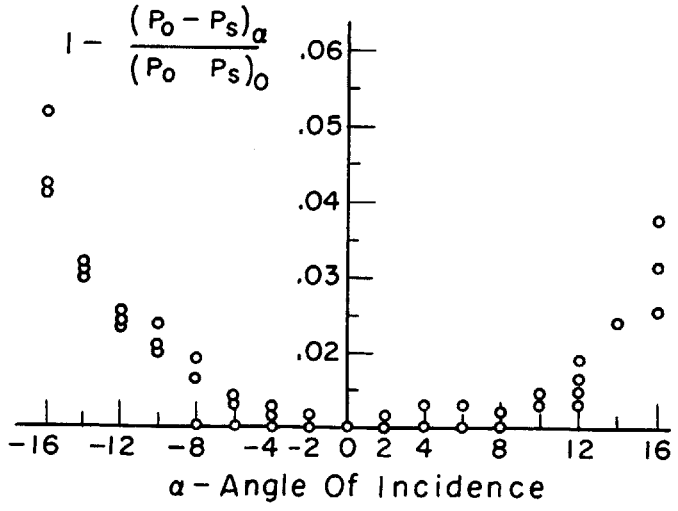

FIG. 12 TOTAL PRESSURE ERROR

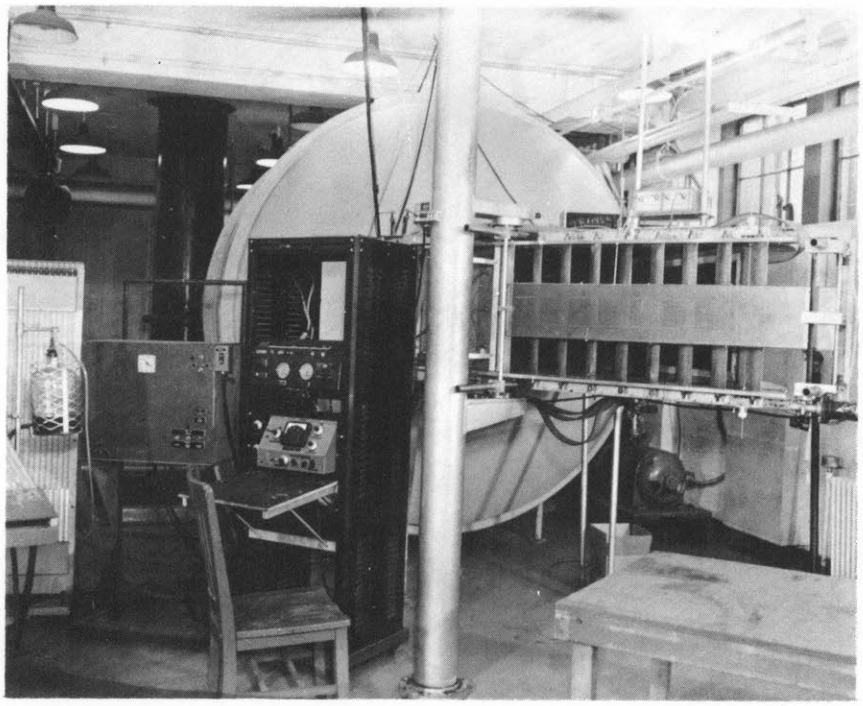

Fig. 13

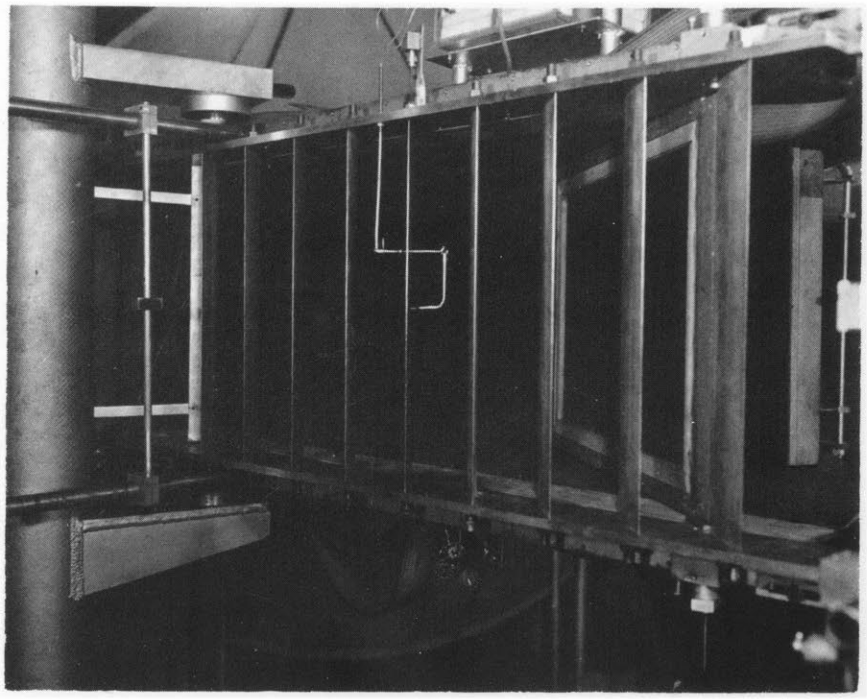

Fig. 14

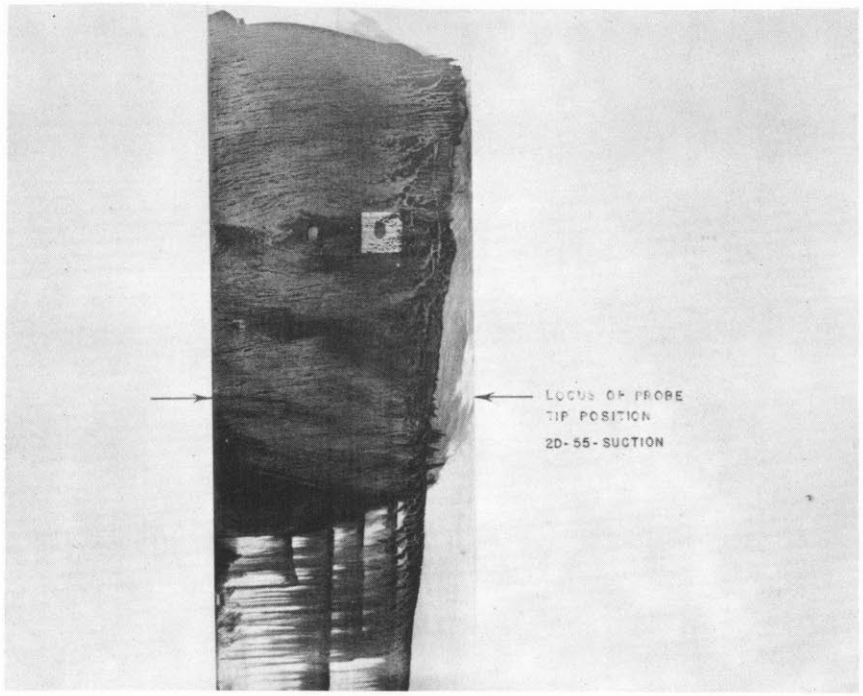
LOCUS OF PROBE
TIP POSITION
2D-55-SUCTION

Fig. 15

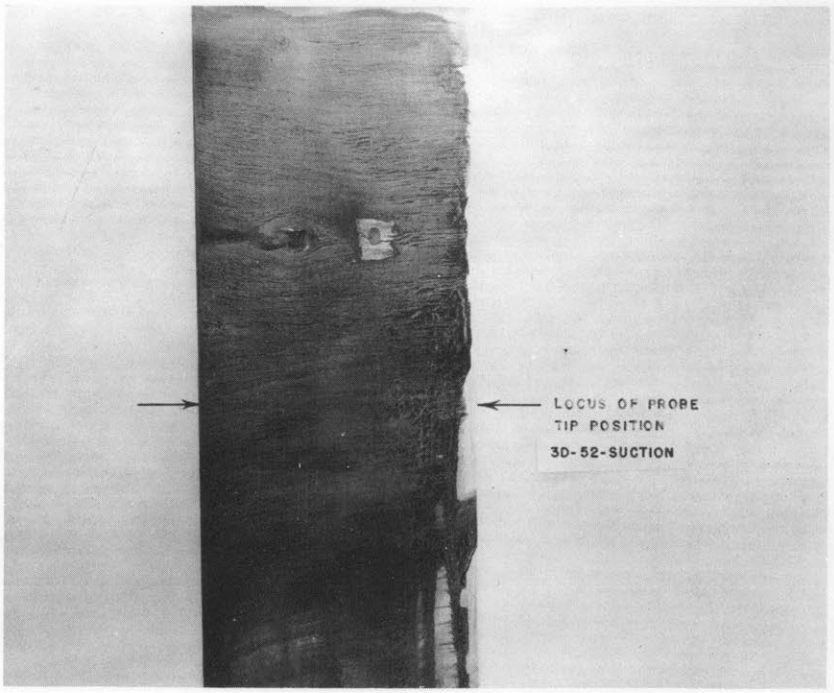
LOCUS OF PROBE
TIP POSITION
3D-52-SUCTION

Fig. 16